

GedankenNet: Self-supervised learning of hologram reconstruction using physics consistency

Luzhe Huang^{1,2,3,*}, Hanlong Chen^{1,2,3,*}, Tairan Liu^{1,2,3}, Aydogan Ozcan^{1,2,3,4}

1 Electrical and Computer Engineering Department, University of California, Los Angeles, CA 90095, USA

2 Bioengineering Department, University of California, Los Angeles, CA 90095, USA

3 California NanoSystems Institute (CNSI), University of California, Los Angeles, CA 90095, USA.

4 David Geffen School of Medicine, University of California Los Angeles, Los Angeles, CA 90095, USA

Corresponding author: ozcan@ucla.edu

* These authors contributed equally to this work

Abstract

The past decade has witnessed transformative applications of deep learning in various computational imaging, sensing and microscopy tasks. Due to the supervised learning schemes employed, most of these methods depend on large-scale, diverse, and labeled training data. The acquisition and preparation of such training image datasets are often laborious and costly, also leading to biased estimation and limited generalization to new types of samples. Here, we report a self-supervised learning model, termed GedankenNet, that eliminates the need for labeled or experimental training data, and demonstrate its effectiveness and superior generalization on hologram reconstruction tasks. Without prior knowledge about the sample types to be imaged, the self-supervised learning model was trained using a physics-consistency loss and artificial random images that are synthetically generated without any experiments or resemblance to real-world samples. After its self-supervised training, GedankenNet successfully generalized to experimental holograms of various unseen biological samples, reconstructing the phase and amplitude images of different types of objects using experimentally acquired test holograms. Without access to experimental data or the knowledge of real samples of interest or their spatial features, GedankenNet's self-supervised learning achieved complex-valued image reconstructions that are consistent with the Maxwell's equations, meaning that its output inference and object solutions accurately represent the wave propagation in free-space. This self-supervised learning of image reconstruction tasks opens up new opportunities for various inverse problems in holography, microscopy and computational imaging fields.

Introduction

Recent advances in deep learning have revolutionized computational imaging, microscopy and holography-related fields, with applications in biomedical imaging¹, sensing², diagnostics³ and 3D displays⁴, also achieving benchmark results in various image translation and enhancement tasks, e.g., super-resolution⁵⁻¹⁰, image denoising¹¹⁻¹³ and virtual staining¹⁴⁻¹⁹, among others. The flexibility of deep learning models has also facilitated their widespread use in different imaging modalities, including brightfield^{20,21} and fluorescence microscopy^{8,10,11,13,22-25}. As another important example, digital holographic microscopy (DHM), a label-free imaging technique widely used in biomedical and physical sciences and engineering²⁶⁻³⁵, has also significantly benefitted from deep learning and neural networks^{4,36-45}. Convolutional neural networks (CNNs)^{36-39,41,43,46-48} and recurrent neural networks (RNNs)^{44,49} have been used for holographic image reconstruction, presenting unique advantages over classical phase retrieval algorithms, such as using fewer measurements and achieving an extended depth-of-field. Researchers also explored deep learning-enabled image analysis⁵⁰⁻⁵⁶ and transformations^{15,16,21,57} on holographic images to further leverage the quantitative phase information (QPI) provided by DHM.

In these existing approaches, supervised learning models were utilized, demanding large-scale, high-quality and diverse training datasets (from various sources and types of objects) with annotations and/or ground truth experimental images. For microscopic imaging and holography, in general, such labeled training data can be acquired through classical algorithms that are treated as the ground truth image reconstruction method^{44,45,49}, or through registered image pairs (input vs. ground truth) acquired by different imaging modalities^{8,14,15,21}. These supervised learning methods require significant labor, time, and cost to acquire, align and pre-process the training images, and potentially introduce inference bias,

resulting in limited generalization to new types of objects never seen during the training. Generally speaking, existing supervised learning models demonstrated on microscopic imaging and holography tasks are highly dependent on the training image datasets acquired through experiments, which show variations due to the optical hardware, types of specimens and imaging (sample preparation) protocols. Using labeled simulated data for network training is another possible solution; however, generating simulated data distributions to accurately represent the experimental sample distributions can be complicated and requires prior knowledge of the sample features and/or some initial measurements with the imaging set-up of interest^{6,58-62}. For example, supervised learning-based deep neural networks for hologram reconstruction tasks demonstrated decent *internal* generalization to new samples of the same type as in the training dataset, while their *external* generalization to different sample types or imaging hardware was limited^{36,43,49}.

A common practice to enhance the imaging performance of a supervised model is to apply transfer learning⁴⁹, which trains the learned model on a subset of the *new* test data. However, the features learned through supervised transfer learning using a limited training data distribution, e.g., specific types of samples, do not necessarily advance external generalization to other types of samples, considering that the sample features and imaging set-up may differ significantly in the blind testing phase. Furthermore, transfer learning requires additional labor and time to collect fresh data from the new testing data distribution and finetune the pre-trained model, which might bring practical challenges in different applications.

In addition to these, deep learning-based solutions for inverse problems in computational imaging generally lack the incorporation of explicit physical models in the training phase;

this, in turn, limits the compatibility of the network’s inference with the physical laws that govern the light–matter interactions and wave propagation. Recent studies demonstrated physics-informed neural networks (PINNs)^{63–66}, where a physical loss was formulated to train the network in an unsupervised manner to solve partial differential equations. However, PINN-based methods that can match (or come close to) the performance of supervised learning methods have not been reported yet for solving inverse problems in computational imaging with successful generalization to new types of samples.

Here, we demonstrate the first self-supervised learning (SSL)-based deep neural network for hologram reconstruction, which is trained without any experimental data or prior knowledge of the types or spatial features of the samples. We term it GedankenNet as the self-supervised training of our network model is based on randomly-generated artificial images with no connection or resemblance to real samples at the micro- or macro-scale, and therefore the spatial frequencies and the features of these images do not represent any real-world samples and are not related to any experimental set-up. As illustrated in Fig. 1(a), the self-supervised learning scheme of GedankenNet adapts a *physics-consistency* loss between the input synthetic holograms of random, artificial objects, and the numerically predicted holograms calculated using the GedankenNet output complex fields, without any reference to or use of the ground truth object fields during the learning process. After its training, the self-supervised GedankenNet directly generalizes to experimental holograms of various types of samples even though it never saw any experimental data or used any information regarding the real samples. When blindly tested on experimental holograms of human tissue sections (lung, prostate and salivary gland tissue) and Pap smears, GedankenNet achieved better image reconstruction accuracy compared to supervised learning models using the same training datasets. We further demonstrated that GedankenNet can be widely applied to other

training datasets, including simulations and experimental datasets, and achieves superior generalization to unseen data distributions over supervised learning-based models.

Since GedankenNet's self-supervised learning is based on a physics-consistency loss, its inference and the resulting output complex fields are compatible with the Maxwell's equations and accurately reflect the physical wave propagation phenomenon in free-space. By testing GedankenNet with experimental input holograms captured at shifted (unknown) axial positions, we showed that GedankenNet does not hallucinate and the object field at the sample plane can be accurately retrieved through wave propagation of the GedankenNet output field, without the need for retraining or finetuning its parameters. These results indicate that in addition to generalizing to experimental holograms of unseen sample types without seeing any experimental data or real object features, GedankenNet also implicitly acquired the physical information of wave propagation in free-space through the same self-supervised learning process.

The success of GedankenNet eliminates three major challenges in existing deep learning-based holographic imaging approaches: (1) the need for large-scale, diverse and labeled training data, (2) the limited generalization to unseen sample types or shifted input data distributions, and (3) the lack of an interpretable connection and compatibility between the physical laws/models and the trained deep neural network. This work introduces a promising and powerful alternative to a wide variety of supervised learning-based methods that are currently applied in various microscopy, holography and computational imaging tasks.

Results

The hologram reconstruction task, in general, can be formulated as an inverse problem⁴²:

$$\hat{o} = \arg \min_o L(H(o), i) + R(o)$$

where $i \in \mathbb{R}^{MN^2}$ represents the vectorized M measured holograms, each of which is of dimension $N \times N$ and $o \in \mathbb{C}^{N^2}$ is the vectorized object complex field. $H(\cdot)$ is the forward imaging model, $L(\cdot)$ is the loss function and $R(\cdot)$ is the regularization term. Under spatially and temporally coherent illumination of a thin sample, $H(\cdot)$ can be simplified as:

$$H(o) = f(Ho) + \epsilon$$

where $H \in \mathbb{C}^{MN^2 \times N^2}$ is the free-space transformation matrix^{42,67}, $\epsilon \in \mathbb{R}^{MN^2}$ represents random detection noise and $f(\cdot)$ refers to the (opto-electronic) sensor-array sampling function, which records the intensity of the optical field.

Different schemes for solving holographic imaging inverse problems are summarized in Fig.

1. Existing methods for generalizable hologram reconstruction can be mainly classified into two categories, as shown in Fig. 1(a): (1) iterative phase retrieval algorithms based on the physical forward model and iterative error-reduction; (2) supervised deep learning-based inference methods that learn from training image pairs of input holograms i and the ground truth object fields o . Similar to the iterative phase recovery algorithms listed under (1), deep neural networks were also used to provide iterative approximations to the object field from a batch of hologram(s); however, these network models were iteratively optimized for each hologram batch separately, and cannot generalize to reconstruct holograms of other objects once they are optimized^{68,69} (see Supplementary Note 1 and Extended Data Fig. 2).

Different from existing learning-based approaches, instead of directly comparing the output complex fields (\hat{o}) and the ground truth object complex fields (o), GedankenNet infers the predicted holograms \hat{i} from its output complex fields \hat{o} using a deterministic physical forward model, and directly compares \hat{i} with i . Without the need to know the ground truth object

fields o , this forward model – network cycle establishes a physics-consistency loss ($L_{physics-consistency}$) for gradient back-propagation and network parameter updates, which is defined as:

$$L_{physics-consistency}(\hat{i}, i) = \alpha L_{FDMAE}(\hat{i}, i) + \beta L_{MSE}(\hat{i}, i),$$

where L_{FDMAE} and L_{MSE} are the Fourier domain mean absolute error (FDMAE) and the mean square error (MSE), respectively, calculated between the input holograms i and the predicted holograms \hat{i} . α, β refer to the corresponding weights of each term (see the Methods section for the training and implementation details). The network architecture of GedankenNet is also detailed in the Methods section and Extended Data Fig. 1.

As emphasized in Fig. 1, GedankenNet eliminates the need for experimental, labeled training data and thus presents unique advantages over existing methods. The training dataset of GedankenNet only consists of artificial holograms generated from random images (with no connection or resemblance to real-world samples), which serve as the amplitude and phase channels of the object field (see the Methods section and Fig. 1(b)). After its self-supervised training using artificial images without any experimental data or real-world specimens, GedankenNet can be directly used to reconstruct experimental holograms of various microscopic specimens, including e.g., densely connected tissue samples and Pap smears. This is vastly in contrast to existing supervised learning methods that exhibit limited external generalization to unseen data distributions and new sample types. Furthermore, compared with classical iterative phase retrieval algorithms, GedankenNet (after its one-time training is complete) provides significantly faster reconstructions for any arbitrary hologram in a single forward inference without the need for numerical iterations, transfer learning or finetuning of its parameters on new testing samples.

To demonstrate these unique features of GedankenNet, we trained a series of self-supervised network models that take multiple input holograms (M ranging from 2 to 7), following the training process introduced in Fig. 1. Each GedankenNet model for a different M value was trained using artificial holograms generated from random synthetic images based on M different planes with designated sample-to-sensor distances $z_i, i = 1, 2, \dots, M$. In the blind testing phase illustrated in Fig. 2(a), M experimental holograms of human lung tissue sections were captured by a lensfree in-line holographic microscope (see Extended Data Fig. 1(b) and the Methods section for experimental details). We tested all the self-supervised GedankenNet models on 94 non-overlapping fields-of-view (FOVs) of tissue sections and quantified the image reconstruction quality in terms of the amplitude and phase structural similarity index measure (SSIM) values with respect to the ground truth object fields (see Fig. 2(b)). The ground truth fields were retrieved by the multi-height phase retrieval (MHPR⁷⁰⁻⁷²) algorithm using $M = 8$ raw holograms of each FOV. Our results indicate that all the GedankenNet models were able to reconstruct the sample fields with high fidelity even though they were trained using random, artificial images without any experimental data (Fig. 2).

We also compared the generalization performance of self-supervised GedankenNet models against other supervised learning models and iterative phase recovery algorithms using experimental holograms of various types of human tissue sections and Pap smears; see Fig. 3. Though only seeing artificial holograms of random images in the training phase, GedankenNet ($M = 2$) was able to directly generalize to experimental holograms of Pap smears and human lung, salivary gland and prostate tissue sections. For comparison, we trained two supervised learning models using the same artificial image dataset, including the Fourier Imager Network (FIN)⁴⁵ and a modified U-Net⁷³ architecture (see the Methods section). These supervised models were tested on the same experimental holograms to

analyze their external generalization performance. Compared to these supervised learning methods, GedankenNet exhibited superior external generalization on all four types of samples (lung, salivary gland and prostate tissue sections and Pap smears), scoring higher enhanced correlation coefficient (ECC) values (see the Methods section). A second comparative analysis was performed against a classical iterative phase recovery method, i.e., MHPR⁷⁰⁻⁷²: GedankenNet inferred the object fields with less noise and higher image fidelity compared to MHPR ($M=2$) that used the same input holograms (see Fig. 3(a,c)). In addition, we compared GedankenNet image reconstruction results against deep image prior (DIP) based approaches^{68,69,74}, also confirming its superior performance (see Extended Data Fig. 2 and Supplementary Note 1).

The inference time of each of these hologram reconstruction algorithms is summarized in Extended Data Table 1, which indicates that GedankenNet accelerated the image reconstruction process by ~ 128 times compared to MHPR ($M=2$). These holographic imaging experiments and resulting analyses successfully demonstrate GedankenNet's unparalleled generalization to experimental holograms of unknown, new types of samples without any prior knowledge about the samples or the use of experimental training data or labels.

In addition to GedankenNet's superior external generalization (from artificial random images to experimental holographic data), this framework can also be applied to other training datasets. To showcase this, we trained three GedankenNet models using (i) the artificial hologram dataset generated from random images, same as before; (ii) a new artificial hologram dataset generated from a natural image dataset (COCO)⁷⁵; (iii) an experimental hologram dataset of human tissue sections (see Methods for dataset preparation). Each one of these training datasets had ~ 100 K training image pairs with $M = 2$, $z_1 = 300 \mu\text{m}$ and $z_2 =$

375 μm . As shown in Fig. 4, these three individually trained GedankenNet models were tested on four testing datasets, including artificial holograms of (1) random synthetic images and (2) natural images as well as experimental holograms of (3) lung tissue sections and (4) Pap smears. Our results reveal that all the self-supervised GedankenNet models showed very good reconstruction quality for both internal and external generalization; see Fig. 4(a-b).

When trained using the experimental holograms of lung tissue sections, the supervised hologram reconstruction model FIN scored higher ECC values than the GedankenNet on the same testing set of the lung tissue sections. However, when it comes to external generalization, as shown in Fig. 4(b), GedankenNet (the blue shadow bar) achieved superior imaging performance compared to FIN (the red shadow bar) on natural images (from COCO dataset). One can also notice the overfitting of the supervised model (FIN) by the large performance gap observed between its internal and external generalization performance shown with the red bars in Fig. 4(b). On the contrary, the self-supervised GedankenNet trained with artificial random images (the blue bars) showed very good generalization performance for both test datasets covering natural macro-scale images as well as micro-scale tissue images.

GedankenNet's strong external generalization is due to its self-supervised learning scheme that employs a physics-consistency loss, which is further validated by the additional comparisons we performed between self-supervised learning and supervised learning schemes; see Extended Data Fig. 3 and Supplementary Note 2. In this new analysis, we compared GedankenNet and the supervised learning model FIN that were trained with the same artificial hologram datasets generated from random synthetic images (Extended Data Fig. 3a) or natural images from COCO dataset (Extended Data Fig. 3b). The blind testing of these models used experimental holograms of Pap smear samples and lung tissue sections.

The results of this comparison (summarized in Extended Data Fig. 3) reveal that the self-supervised learning scheme consistently achieved better reconstruction accuracy and enhanced ECC scores over the supervised learning scheme, further highlighting the superior external generalization of GedankenNet to experimental holograms of new types of samples.

Besides its generalization to unseen testing data distributions and experimental holograms, the inference of GedankenNet is also compatible with the wave equation. To demonstrate this, we tested the GedankenNet model (trained with the artificial hologram dataset generated from random synthetic images) on experimental holograms captured at shifted unknown axial positions $z'_1 \cong z_1 + \Delta z$ and $z'_2 \cong z_2 + \Delta z$, where z_1, z_2 were the training axial positions and Δz is the unknown axial shift amount. The same model as in Fig. 3 was used for this analysis and blindly tested on lung tissue sections (i.e., external generalization). Due to the unknown axial defocus distance (Δz), the direct output fields of GedankenNet do not match well with the ground truth, indicated by the orange curve in Fig. 5. However, since GedankenNet was trained with the physics-consistency loss, its output fields are compatible with the wave equation in free-space. Thus, the object fields at the sample plane can be accurately retrieved from the GedankenNet output fields by performing wave propagation by the corresponding axial defocus distance. After propagating the output fields of GedankenNet by $-\Delta z$ using the angular spectrum approach, the propagated fields (blue curve) matched very well with the ground truth fields across a large range of axial defocus values, Δz . These results are important because (1) they once again demonstrate the success of GedankenNet in generalizing to experimental holograms even though it was only trained by artificial holograms of random synthetic images; and (2) the physics-consistency based self-supervised training of GedankenNet encoded the wave equation into its inference process so that instead of hallucinating and creating non-physical random optical fields when tested with defocused

holograms, GedankenNet outputs correct (physically consistent) defocused complex fields. In this sense, GedankenNet not only exhibits superior external generalization (from experiment- and data-free training to experimental holograms), but also very well generalized to work with arbitrarily defocused experimental holograms. To the best of our knowledge, these features were not demonstrated before for any hologram reconstruction neural network in the literature.

The self-supervised experiment-free learning scheme of GedankenNet also brings robustness to perturbations caused by the imaging hardware, such as e.g., limited signal-to-noise ratio (SNR) or optical aberrations. In Fig. 6, we validated this robustness of GedankenNet to data perturbations, modeled as random measurement noise in the forward imaging model. For this analysis, we trained GedankenNet and a supervised deep neural network model (FIN) using the artificial hologram dataset generated from random synthetic images, the same as before. The trained models were then tested on artificial holograms generated from natural macro-scale images (COCO dataset) with different levels of white Gaussian noise added, as shown in Fig. 6(b). Figure 6(c) illustrates the hologram reconstruction results of both models (GedankenNet vs. supervised learning-based FIN); Fig. 6(e) further compares the root mean square error (RMSE) values for the amplitude and phase channels, as well as the ECC values of these reconstructions. The results revealed that GedankenNet hologram reconstruction quality relatively degraded with input holograms having more noise (lower SNR), but its performance was still superior compared to the supervised learning-based FIN model trained on the same artificial hologram dataset. Additionally, we tested another supervised FIN model (trained on experimental holograms of lung tissue sections, i.e., the same model used in Fig. 4) on the same simulated test holograms and summarized its inference outputs in Fig. 6(d). Compared to the other two models trained on the artificial hologram dataset, the

experimental-data-driven supervised FIN model exhibited inferior reconstruction quality and lower ECC values for unseen object features, demonstrating significantly poorer external generalization. In general, supervised hologram reconstruction models overfit to perturbations or noise present in their training, which makes them more susceptible to unseen perturbations from other sources or lower SNR input holograms compared to their training data. This superior generalization of GedankenNet to poor SNR input holograms (Fig. 6) stems from its self-supervised learning using the physical-consistency loss and artificial holograms, as opposed to directly learning a mapping between the input and the target image domains through experimental data.

Discussion

In this work, we demonstrated GedankenNet, a self-supervised hologram reconstruction neural network that eliminates the dependence on labeled and experimental training data, and achieves better generalization to unseen data distributions than existing methods. Based on its self-supervised learning scheme and the physics-consistency loss function, GedankenNet is able to implicitly learn the physics of wave propagation and perform hologram reconstruction tasks without any experimental data or prior knowledge of the samples. Stated differently, the training of GedankenNet involves *Gedankenexperiments* (thought experiments) without involving any experimental data or any prior knowledge about real-world samples, and after its training, GedankenNet successfully generalizes to experimental holograms and shows superior reconstruction quality for external generalization compared with supervised learning-based network models. We also demonstrated that GedankenNet outputs are compatible with the wave equation, and it does not hallucinate artificial (non-physical) output fields when defocused holograms are provided as input. These results present an additional degree of successful generalization (beyond experiment- and data-free training to

experimental holograms) since during the self-supervised training of GedankenNet we always used $\Delta z = 0$.

Compared with the existing supervised learning methods, GedankenNet has several unique advantages. It eliminates the dependence on labeled experimental training data in computational microscopy, which often come from other imaging modalities or classical algorithms and therefore, inevitably introduce biases for external generalization performance of the trained network. The self-supervised learning scheme of GedankenNet also considerably relieves the cost and labor of collecting and preparing large-scale microscopic image datasets. Limited by the optical system, the experimental holographic imaging process applies a low-pass filter to the ground truth object fields. Furthermore, the recurrent spatial features within the same type of samples further reduce the diversity of the experimental datasets. Thus, adapting simulated holograms of random, artificial image datasets presents a more effective solution when access to large amounts of experimental data is impractical. In addition, GedankenNet exhibits superior generalization to unseen data distributions than supervised models, and achieves better holographic image reconstruction for unseen, new types of samples (see e.g., Figs. 3-4).

During the training phase of GedankenNet, the physical forward model is given to the network as part of the *Gedankenexperiments*. However, perturbations, i.e., the mismatch between the *a priori* forward model and the *a posteriori* model in the experiments, could impact the performance of the learned GedankenNet. These sources of perturbations often include: (1) the measurement noise ϵ , (2) the modeling error of the sampling function f and (3) the error of the transfer function H . The first two sources can come from a combination of factors, e.g., thermal and shot noise, sensor nonlinearity, aberrations, etc., and can be

properly handled by setting regularization terms in the loss function, e.g., the total variation (TV) loss⁷⁶. The last source of perturbations may result from the assumptions when establishing the forward model and errors in the key parameters of the holographic imaging system, e.g., the sample-to-sensor distances, the illumination wavelength, etc. In fact, self-supervised models are shown to be more robust to adversarial attacks and input image/data corruptions and exceed the performance of fully supervised models on near-distribution outliers^{77,78}.

In summary, GedankenNet overcomes important limitations of existing deep learning models in holographic microscopy by creating experimental-data-free, generalizable, and physics-compatible deep learning models. GedankenNet further opens up new opportunities for other microscopy imaging modalities and various computational inverse imaging problems and could facilitate a diverse set of applications for deep learning-based holography and microscopy techniques.

Figures and figure legends

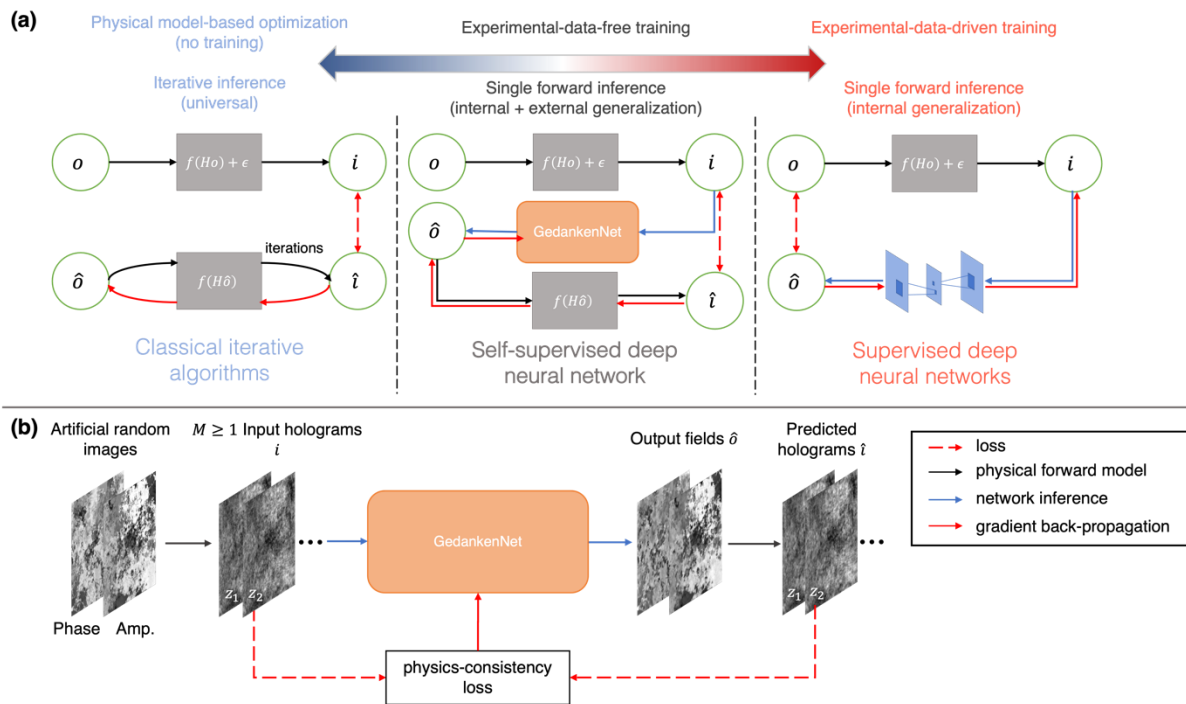


Figure 1. Diagrams of GedankenNet and other existing methods for solving holographic imaging problems. (a) Diagrams of classical iterative hologram reconstruction algorithms, the self-supervised deep neural network (GedankenNet) and existing supervised deep neural networks. (b) Self-supervised training pipeline of GedankenNet for hologram reconstruction.

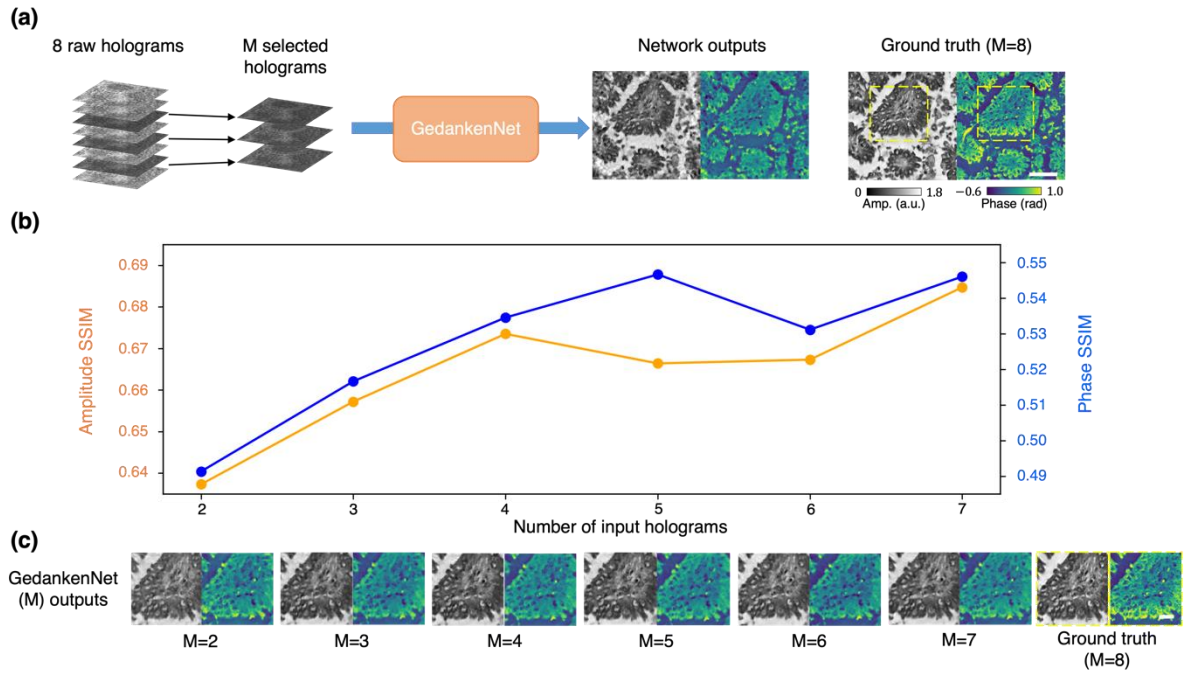


Figure 2. Hologram reconstruction performance of GedankenNet using multiple (M) input holograms. (a) M holograms were selected from 8 raw holograms as the inputs for GedankenNet. The ground truth complex field (used only for comparison) was retrieved by MHPR using all the 8 raw holograms. Scale bar: 50 μm . (b) The amplitude and phase SSIM values between the reconstructed fields of GedankenNet and the ground truth object fields. SSIM values were averaged on a testing set with 94 unique human lung tissue FOVs. (c) Zoomed-in regions of the GedankenNet outputs and the ground truth object fields. Scale bar: 20 μm .

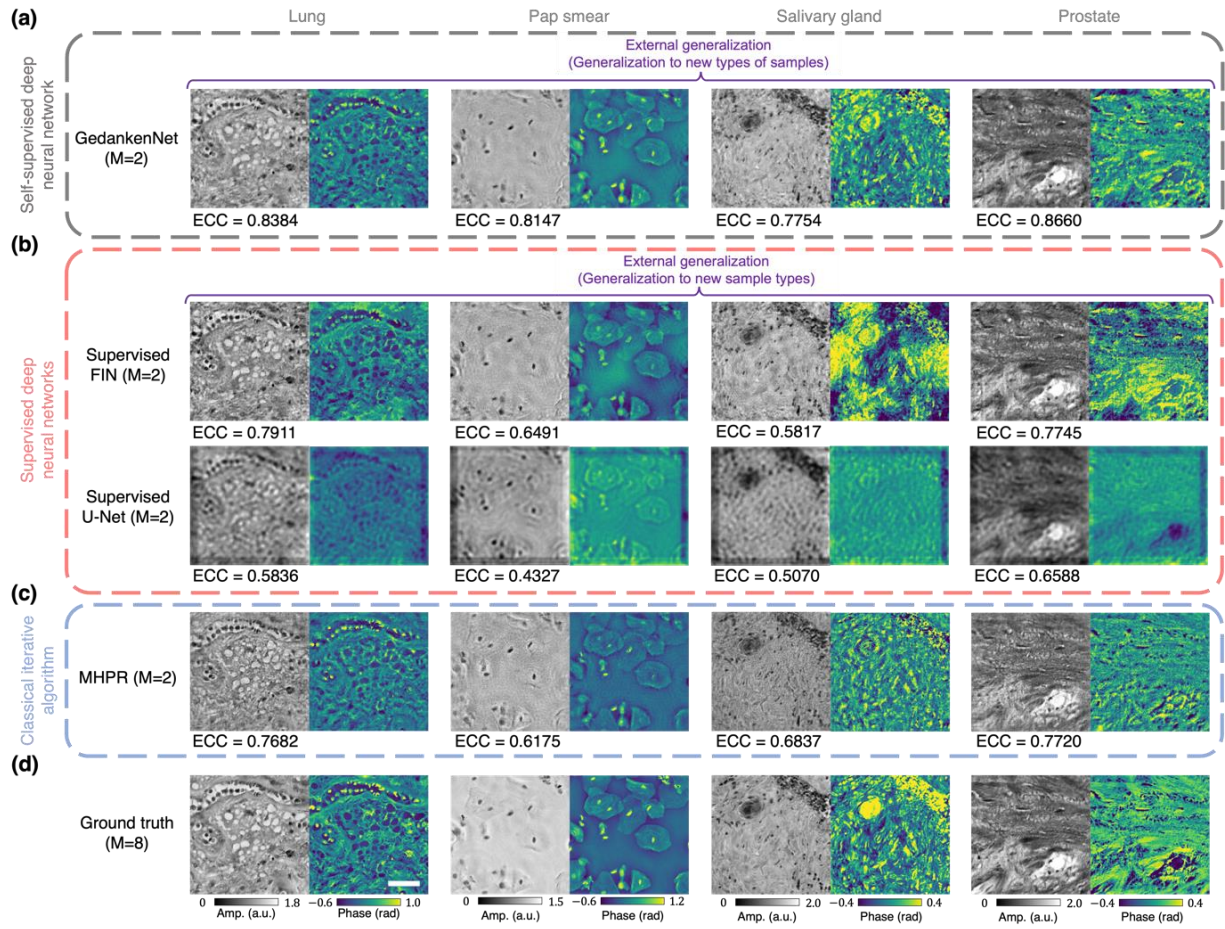


Figure 3. External generalization of GedankenNet on human tissue sections and Pap smears, and its comparison with existing supervised learning models and MHPR. (a) External generalization results of GedankenNet on human lung, salivary gland and Pap smear holograms. (b) External generalization results of supervised learning methods on the same test datasets. The supervised models were trained on the same simulated hologram dataset as GedankenNet used. (c) MHPR reconstruction results using the same $M = 2$ input holograms. (d) Ground truth object fields retrieved using 8 raw holograms of each FOV. Scale bar: 50 μm .

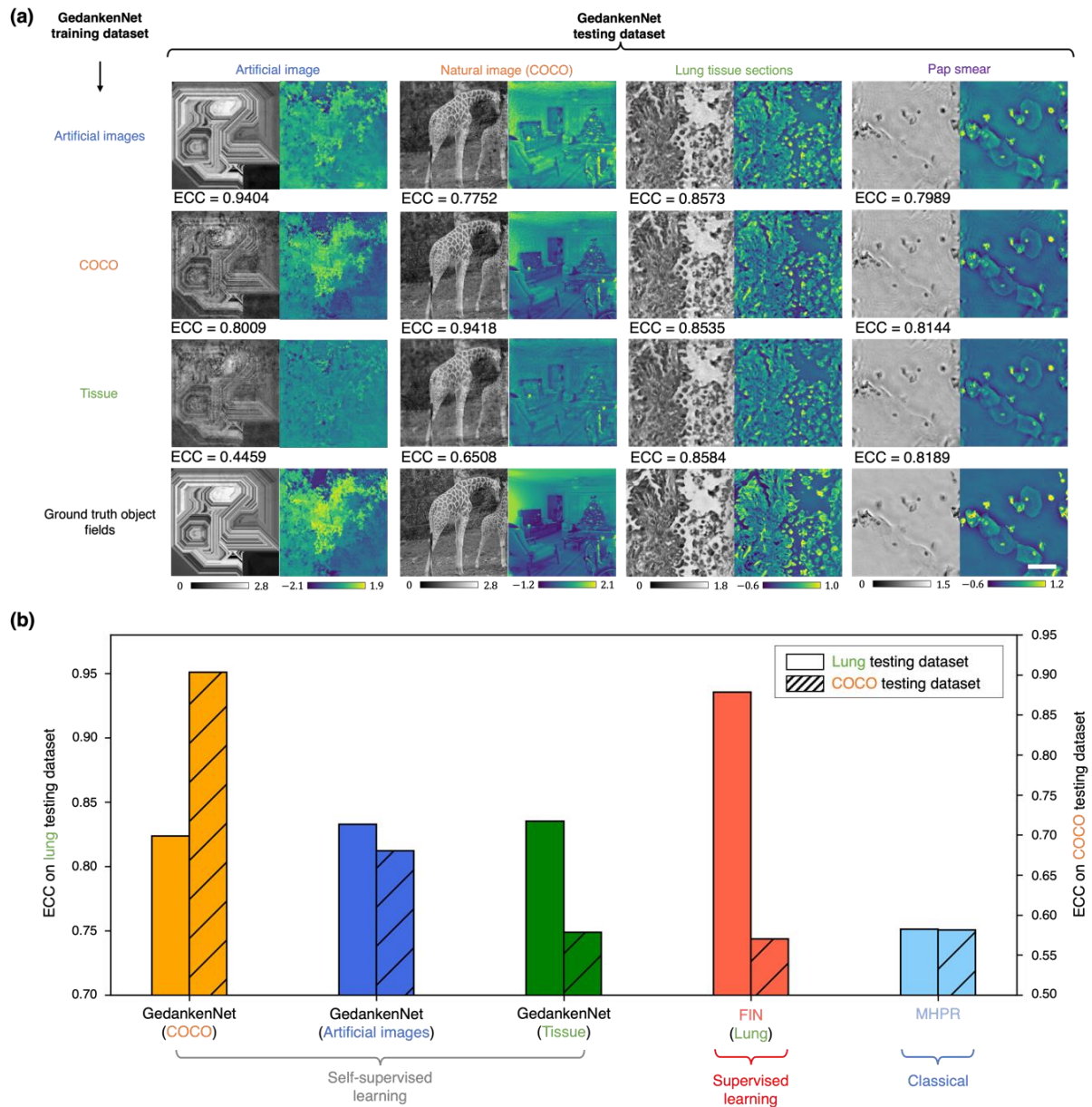


Figure 4. Generalization of GedankenNet trained with different training datasets to various new testing datasets. (a) Outputs of GedankenNet models trained on three different training datasets (artificially generated random synthetic images, natural images (COCO) and tissue sections, respectively). (b) Quantitative performance analysis of GedankenNet models trained on three different datasets. The performances of a supervised deep neural network (trained on lung tissue sections) and MHPR are also included for comparison purposes. ECC values were averaged on lung and COCO test datasets with 94 and 100 unique FOVs, respectively. Scale bar: 50 μm .

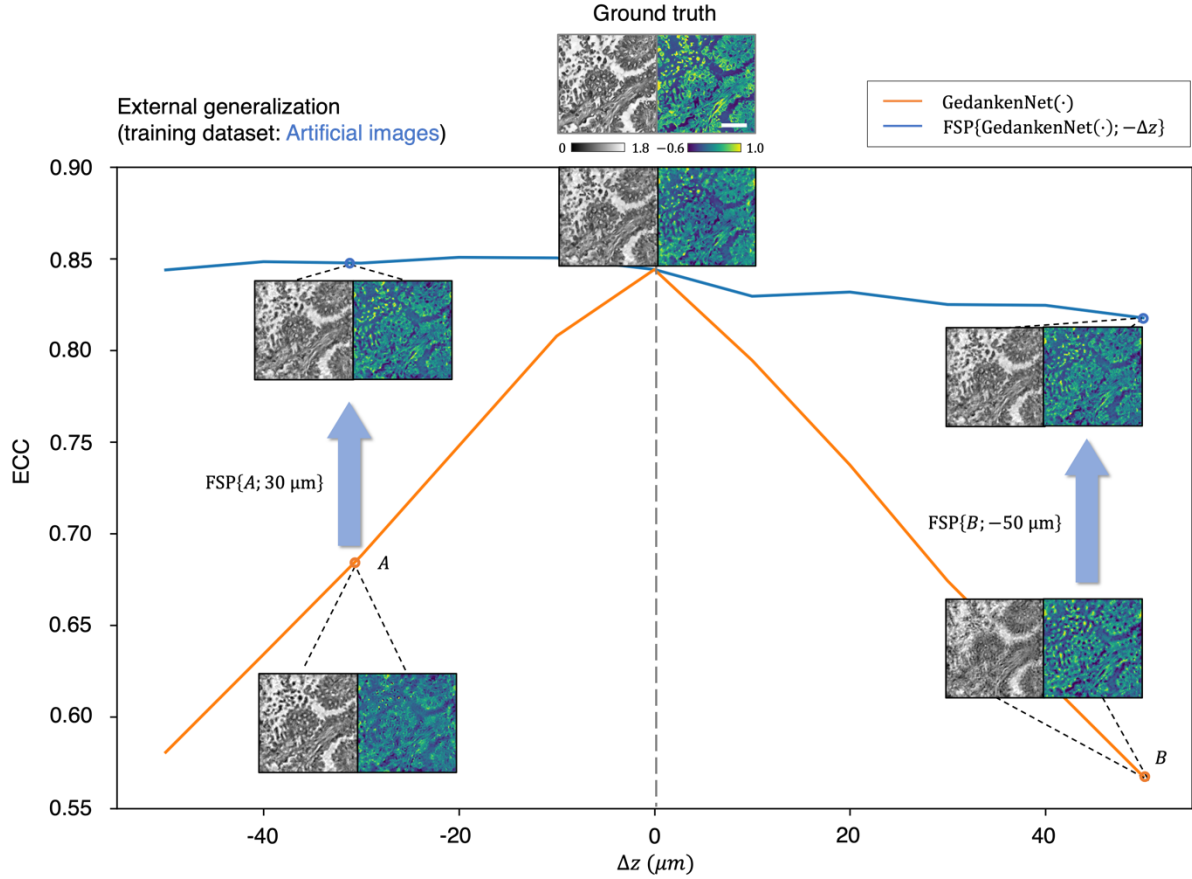


Figure 5. Compatibility of GedankenNet output images with the wave equation in free-space. GedankenNet model was trained to reconstruct $M = 2$ input holograms at $z_1 = 300\mu\text{m}$ and $z_2 = 375\mu\text{m}$, but blindly tested on input holograms captured at $z'_1 = 300 + \Delta z \mu\text{m}$, $z'_2 = 375 + \Delta z \mu\text{m}$. The resulting GedankenNet output complex fields are propagated in free-space by $-\Delta z$ using the wave equation, revealing a very good image quality (blue curve) across a wide range of axial defocus distances. These results demonstrate that GedankenNet not only has a superior external generalization to experimental holograms (using experiment- and data-free training), but also very well generalized to work with arbitrarily defocused experimental holograms, and encoded the wave equation into its inference process using the physics-consistency loss. Scale bar: $50 \mu\text{m}$.

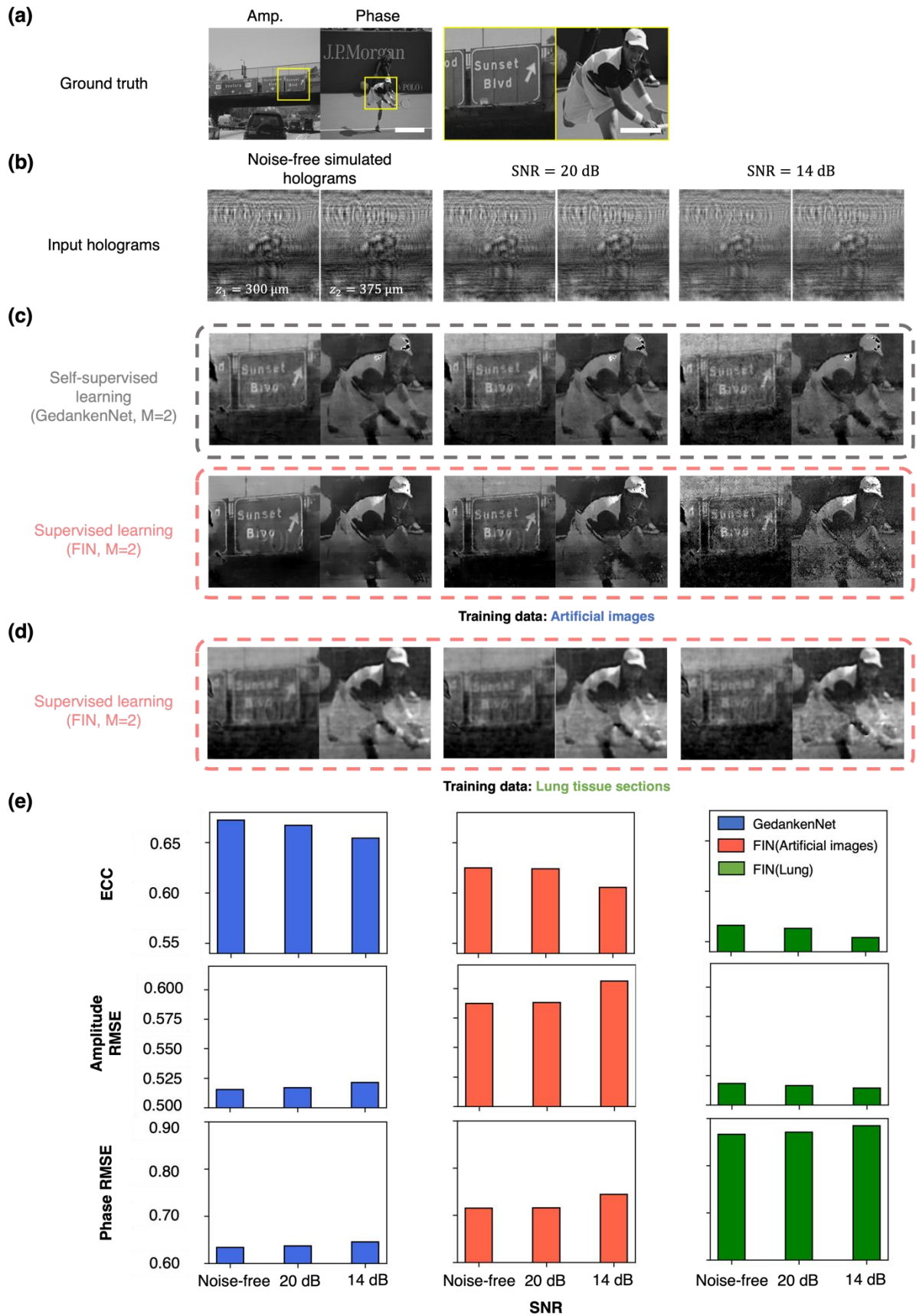


Figure 6. SNR comparison between GedankenNet and a supervised deep neural network

FIN. (a) The ground truth object fields and the zoomed-in regions marked by the yellow boxes. (b) Simulated holograms using natural images (from COCO dataset) with and without the presence of random noise. The noise-added holograms have 20 dB and 14 dB SNR, respectively. (c) The zoomed-in outputs of GedankenNet and FIN inference on the simulated test holograms shown in (b). Both models shared the same artificial hologram training dataset (generated from random images) and the same network architecture. (d) The zoomed-in outputs of another supervised FIN model (trained using the experimental lung tissue holograms) blindly tested on the same simulated test holograms shown in (b). (e) Quantitative performance comparisons of GedankenNet and supervised FIN models. Metrics were averaged using 100 unique FOVs. Scale bar: 50 μm , 20 μm for zoomed-in images.

References

1. Suzuki, K. Overview of deep learning in medical imaging. *Radiol. Phys. Technol.* **10**, 257–273 (2017).
2. Ma, L. *et al.* Deep learning in remote sensing applications: A meta-analysis and review. *ISPRS J. Photogramm. Remote Sens.* **152**, 166–177 (2019).
3. Bakator, M. & Radosav, D. Deep Learning and Medical Diagnosis: A Review of Literature. *Multimodal Technol. Interact.* **2**, 47 (2018).
4. Shimobaba, T. *et al.* Deep-Learning Computational Holography: A Review (Invited). *Front. Photonics* **3**, 854391 (2022).
5. Rivenson, Y. *et al.* Deep learning microscopy. *Optica* **4**, 1437 (2017).
6. Nehme, E., Weiss, L. E., Michaeli, T. & Shechtman, Y. Deep-STORM: super-resolution single-molecule microscopy by deep learning. *Optica* **5**, 458 (2018).
7. Ouyang, W., Aristov, A., Lelek, M., Hao, X. & Zimmer, C. Deep learning massively accelerates super-resolution localization microscopy. *Nat. Biotechnol.* **36**, 460–468 (2018).
8. Wang, H. *et al.* Deep learning enables cross-modality super-resolution in fluorescence microscopy. *Nat. Methods* **16**, 103–110 (2019).
9. Liu, T. *et al.* Deep learning-based super-resolution in coherent imaging systems. *Sci. Rep.* **9**, 3926 (2019).
10. Qiao, C. *et al.* Evaluation and development of deep neural networks for image super-resolution in optical microscopy. *Nat. Methods* **18**, 194–202 (2021).
11. Weigert, M. *et al.* Content-aware image restoration: pushing the limits of fluorescence microscopy. *Nat. Methods* **15**, 1090–1097 (2018).
12. de Haan, K., Rivenson, Y., Wu, Y. & Ozcan, A. Deep-Learning-Based Image Reconstruction and Enhancement in Optical Microscopy. *Proc. IEEE* **108**, 30–50 (2020).

13. Chen, J. *et al.* Three-dimensional residual channel attention networks denoise and sharpen fluorescence microscopy image volumes. *Nat. Methods* **18**, 678–687 (2021).
14. Rivenson, Y. *et al.* Virtual histological staining of unlabelled tissue-autofluorescence images via deep learning. *Nat. Biomed. Eng.* **3**, 466–477 (2019).
15. Rivenson, Y. *et al.* PhaseStain: the digital staining of label-free quantitative phase microscopy images using deep learning. *Light Sci. Appl.* **8**, 23 (2019).
16. Nygate, Y. N. *et al.* Holographic virtual staining of individual biological cells. *Proc. Natl. Acad. Sci.* **117**, 9223–9231 (2020).
17. Zhang, Y. *et al.* Digital synthesis of histological stains using micro-structured and multiplexed virtual staining of label-free tissue. *Light Sci. Appl.* **9**, 78 (2020).
18. Liu, Y., Yuan, H., Wang, Z. & Ji, S. Global Pixel Transformers for Virtual Staining of Microscopy Images. *IEEE Trans. Med. Imaging* **39**, 2256–2266 (2020).
19. de Haan, K. *et al.* Deep learning-based transformation of H&E stained tissues into special stains. *Nat. Commun.* **12**, 4884 (2021).
20. Rivenson, Y. *et al.* Deep Learning Enhanced Mobile-Phone Microscopy. *ACS Photonics* **5**, 2354–2364 (2018).
21. Wu, Y. *et al.* Bright-field holography: cross-modality deep learning enables snapshot 3D imaging with bright-field contrast using a single hologram. *Light Sci. Appl.* **8**, 25 (2019).
22. Wu, Y. *et al.* Three-dimensional virtual refocusing of fluorescence microscopy images using deep learning. *Nat. Methods* **16**, 1323–1331 (2019).
23. Luo, Y., Huang, L., Rivenson, Y. & Ozcan, A. Single-Shot Autofocusing of Microscopy Images Using Deep Learning. *ACS Photonics* **8**, 625–638 (2021).
24. Xiong, H. *et al.* Super-resolution vibrational microscopy by stimulated Raman excited fluorescence. *Light Sci. Appl.* **10**, 87 (2021).

25. Huang, L., Chen, H., Luo, Y., Rivenson, Y. & Ozcan, A. Recurrent neural network-based volumetric fluorescence microscopy. *Light Sci. Appl.* **10**, 62 (2021).
26. Mudanyali, O. *et al.* Compact, light-weight and cost-effective microscope based on lensless incoherent holography for telemedicine applications. *Lab. Chip* **10**, 1417–1428 (2010).
27. Popescu, G. *Quantitative phase imaging of cells and tissues*. (McGraw-Hill, 2011).
28. Osten, W. *et al.* Recent advances in digital holography [Invited]. *Appl. Opt.* **53**, G44 (2014).
29. Memmolo, P. *et al.* Recent advances in holographic 3D particle tracking. *Adv. Opt. Photonics* **7**, 713 (2015).
30. Merola, F. *et al.* Tomographic flow cytometry by digital holography. *Light Sci. Appl.* **6**, e16241–e16241 (2017).
31. Wu, Y. & Ozcan, A. Lensless digital holographic microscopy and its applications in biomedicine and environmental monitoring. *Methods* **136**, 4–16 (2018).
32. Paturzo, M. *et al.* Digital Holography, a metrological tool for quantitative analysis: Trends and future applications. *Opt. Lasers Eng.* **104**, 32–47 (2018).
33. Park, Y., Depeursinge, C. & Popescu, G. Quantitative phase imaging in biomedicine. *Nat. Photonics* **12**, 578–589 (2018).
34. Javidi, B. *et al.* Roadmap on digital holography [Invited]. *Opt. Express* **29**, 35078 (2021).
35. Balasubramani, V. *et al.* Roadmap on Digital Holography-Based Quantitative Phase Imaging. *J. Imaging* **7**, 252 (2021).
36. Rivenson, Y., Zhang, Y., Günaydın, H., Teng, D. & Ozcan, A. Phase recovery and holographic image reconstruction using deep learning in neural networks. *Light Sci. Appl.* **7**, 17141 (2018).

37. Wu, Y. *et al.* Extended depth-of-field in holographic imaging using deep-learning-based autofocusing and phase recovery. *Optica* **5**, 704–710 (2018).
38. Zhang, G. *et al.* Fast phase retrieval in off-axis digital holographic microscopy through deep learning. *Opt. Express* **26**, 19388–19405 (2018).
39. Wang, K., Dou, J., Kemaq, Q., Di, J. & Zhao, J. Y-Net: a one-to-two deep learning framework for digital holographic reconstruction. *Opt. Lett.* **44**, 4765–4768 (2019).
40. Jo, Y. *et al.* Quantitative Phase Imaging and Artificial Intelligence: A Review. *IEEE J. Sel. Top. Quantum Electron.* **25**, 1–14 (2019).
41. Rivenson, Y., Wu, Y. & Ozcan, A. Deep learning in holography and coherent imaging. *Light Sci. Appl.* **8**, 85 (2019).
42. Barbastathis, G., Ozcan, A. & Situ, G. On the use of deep learning for computational imaging. *Optica* **6**, 921–943 (2019).
43. Deng, M., Li, S., Goy, A., Kang, I. & Barbastathis, G. Learning to synthesize: robust phase retrieval at low photon counts. *Light Sci. Appl.* **9**, 36 (2020).
44. Huang, L. *et al.* Holographic Image Reconstruction with Phase Recovery and Autofocusing Using Recurrent Neural Networks. *ACS Photonics* **8**, 1763–1774 (2021).
45. Chen, H., Huang, L., Liu, T. & Ozcan, A. Fourier Imager Network (FIN): A deep neural network for hologram reconstruction with superior external generalization. *Light Sci. Appl.* **11**, 254 (2022).
46. Goy, A., Arthur, K., Li, S. & Barbastathis, G. Low Photon Count Phase Retrieval Using Deep Learning. *Phys. Rev. Lett.* **121**, 243902 (2018).
47. Ren, Z., Xu, Z. & Lam, E. Y. End-to-end deep learning framework for digital holographic reconstruction. *Adv. Photonics* **1**, 016004 (2019).

48. Byeon, H., Go, T. & Lee, S. J. Deep learning-based digital in-line holographic microscopy for high resolution with extended field of view. *Opt. Laser Technol.* **113**, 77–86 (2019).
49. Huang, L., Yang, X., Liu, T. & Ozcan, A. Few-shot transfer learning for holographic image reconstruction using a recurrent neural network. *APL Photonics* **7**, 070801 (2022).
50. Jo, Y. *et al.* Holographic deep learning for rapid optical screening of anthrax spores. *Sci. Adv.* **3**, e1700606 (2017).
51. Pavillon, N., Hobro, A. J., Akira, S. & Smith, N. I. Noninvasive detection of macrophage activation with single-cell resolution through machine learning. *Proc. Natl. Acad. Sci.* **115**, (2018).
52. Go, T., Kim, J. H., Byeon, H. & Lee, S. J. Machine learning-based in-line holographic sensing of unstained malaria-infected red blood cells. *J. Biophotonics* **11**, e201800101 (2018).
53. Choi, G. *et al.* Cycle-consistent deep learning approach to coherent noise reduction in optical diffraction tomography. *Opt. Express* **27**, 4927 (2019).
54. Ozaki, Y. *et al.* Label-free classification of cells based on supervised machine learning of subcellular structures. *PLOS ONE* **14**, e0211347 (2019).
55. Rubin, M. *et al.* TOP-GAN: Stain-free cancer cell classification using deep learning with a small training set. *Med. Image Anal.* **57**, 176–185 (2019).
56. Chen, L., Chen, X., Cui, H., Long, Y. & Wu, J. Image enhancement in lensless inline holographic microscope by inter-modality learning with denoising convolutional neural network. *Opt. Commun.* **484**, 126682 (2021).
57. Kandel, M. E. *et al.* Phase imaging with computational specificity (PICS) for measuring dry mass changes in sub-cellular compartments. *Nat. Commun.* **11**, 6256 (2020).

58. Boyd, N., Jonas, E., Babcock, H. & Recht, B. DeepLoco: Fast 3D Localization Microscopy Using Neural Networks. *BioRxiv Doi 101101267096* (2018)
doi:10.1101/267096.
59. Zhang, H. *et al.* High-throughput, high-resolution deep learning microscopy based on registration-free generative adversarial network. *Biomed. Opt. Express* **10**, 1044 (2019).
60. Nehme, E. *et al.* DeepSTORM3D: dense 3D localization microscopy and PSF design by deep learning. *Nat. Methods* **17**, 734–740 (2020).
61. Sekh, A. A. *et al.* Physics-based machine learning for subcellular segmentation in living cells. *Nat. Mach. Intell.* **3**, 1071–1080 (2021).
62. Wang, Z. *et al.* Real-time volumetric reconstruction of biological dynamics with light-field microscopy and deep learning. *Nat. Methods* **18**, 551–556 (2021).
63. Raissi, M., Perdikaris, P. & Karniadakis, G. E. Physics-informed neural networks: A deep learning framework for solving forward and inverse problems involving nonlinear partial differential equations. *J. Comput. Phys.* **378**, 686–707 (2019).
64. Karniadakis, A. D. J. & G. E. Extended Physics-Informed Neural Networks (XPINNs): A Generalized Space-Time Domain Decomposition Based Deep Learning Framework for Nonlinear Partial Differential Equations. *Commun. Comput. Phys.* **28**, 2002–2041 (2020).
65. Li, Z. *et al.* Fourier Neural Operator for Parametric Partial Differential Equations. in *2021 Internal Conference on Learning Representations* (2021).
66. Karniadakis, G. E. *et al.* Physics-informed machine learning. *Nat. Rev. Phys.* **3**, 422–440 (2021).
67. Goodman, J. W. *Introduction to Fourier optics*. (Roberts & Co, 2005).
68. Bostan, E., Heckel, R., Chen, M., Kellman, M. & Waller, L. Deep phase decoder: self-calibrating phase microscopy with an untrained deep neural network. *Optica* **7**, 559 (2020).

69. Wang, F. *et al.* Phase imaging with an untrained neural network. *Light Sci. Appl.* **9**, 77 (2020).
70. Greenbaum, A. & Ozcan, A. Maskless imaging of dense samples using pixel super-resolution based multi-height lensfree on-chip microscopy. *Opt. Express* **20**, 3129–3143 (2012).
71. Greenbaum, A. *et al.* Wide-field computational imaging of pathology slides using lens-free on-chip microscopy. *Sci. Transl. Med.* **6**, 267ra175 (2014).
72. Rivenson, Y. *et al.* Sparsity-based multi-height phase recovery in holographic microscopy. *Sci. Rep.* **6**, 37862 (2016).
73. Ronneberger, O., Fischer, P. & Brox, T. U-Net: Convolutional Networks for Biomedical Image Segmentation. *ArXiv150504597 Cs* (2015).
74. Lempitsky, V., Vedaldi, A. & Ulyanov, D. Deep Image Prior. in *2018 IEEE/CVF Conference on Computer Vision and Pattern Recognition* 9446–9454 (IEEE, 2018). doi:10.1109/CVPR.2018.00984.
75. Lin, T.-Y. *et al.* Microsoft COCO: Common Objects in Context. Preprint at <http://arxiv.org/abs/1405.0312> (2015).
76. Rudin, L. I., Osher, S. & Fatemi, E. Nonlinear total variation based noise removal algorithms. *Phys. Nonlinear Phenom.* **60**, 259–268 (1992).
77. Hendrycks, D., Mazeika, M., Kadavath, S. & Song, D. Using Self-Supervised Learning Can Improve Model Robustness and Uncertainty. in *Advances in Neural Information Processing Systems* (eds. Wallach, H. *et al.*) vol. 32 (Curran Associates, Inc., 2019).
78. Liu, H., HaoChen, J. Z., Gaidon, A. & Ma, T. Self-supervised Learning is More Robust to Dataset Imbalance. Preprint at <http://arxiv.org/abs/2110.05025> (2022).